

Pulsar-wind nebulae in X-rays and TeV γ -rays

O. Kargaltsev* and G. G. Pavlov†

*University of Florida, Bryant Space Center, Gainesville, FL 32611, USA

†Pennsylvania State University, 525 Davey Lab., University Park, PA 16802, USA

Abstract. Pulsars are known to be efficient accelerators that produce copious amounts of relativistic particles and inject them into the Galactic medium. The radiation emitted by such a pulsar wind can be seen from radio through γ -rays as a pulsar-wind nebula (PWN). Here we overview and summarize recent progress in X-ray and TeV observations of PWNe.

Keywords: Pulsar Wind Nebulae; Pulsars; Supernova Remnants; Neutron Stars

PACS: 97.60.Gb; 98.38.Mz; 98.38.-j; 98.70.Qy; 97.60.Jd

Along with supernovae and microquasars, pulsars are among the primary sources of the leptonic cosmic rays. The energies of the pulsar wind electrons and positrons range from $\lesssim 1$ GeV to ~ 1 PeV, placing their synchrotron and inverse Compton (IC) emission into radio-X-ray and GeV-TeV bands, respectively. This multiwavelength emission can be seen as a *pulsar-wind nebula* (PWN; see [1] and [2] for reviews). During the last decade, observations with modern X-ray and TeV observatories have dramatically increased the number of known PWNe whose properties are summarized in this review.

As of December 2009, about 60 PWNe associated with known radio or γ -ray pulsars have been detected. We have compiled the properties of these PWNe and their host pulsars in Tables 1 and 2. In most cases we have reanalyzed the X-ray PWN properties to ensure the uniformity of the analysis. The luminosities, spectral slopes, and sizes of the TeV PWNe have been taken from publications as well as from recent conference presentations. Because of the page limit, we mainly discuss the luminosities and, very briefly, spectra and sizes of these PWNe.

We see from Table 2 that the TeV PWN sizes generally increase with pulsar age while the X-ray PWN sizes¹ show an opposite trend. Moreover, for pulsars older than ~ 10 kyr the sizes of the TeV PWNe are typically 100–1000 times larger than the sizes of the X-ray PWNe, while the difference is only a factor of a few for some younger pulsars (e.g., Crab). This suggests that the aged and cooled electrons (mainly seen through their synchrotron emission in radio and IC emission in TeV) have propagated, through advection and/or diffusion, farther away from the pulsar than the recently injected electrons, responsible for the X-ray synchrotron nebulae. While comparing the X-ray and TeV PWNe, one should take into account that larger numbers of electrons have been produced earlier in the pulsar’s life (the electron production rate $\propto \dot{E}(t) \propto \dot{E}_0(1+t/\tau_0)^{-(n+1)/(n-1)}$, where n is the pulsar’s braking index and τ_0 is the initial spin-

¹ Here, while referring to X-ray PWN size, spectrum, or luminosity, we only consider the bright PWN “core” restricted to the torus/arcs regions or the “bullet” in ram pressure confined PWNe (see [2]).

TABLE 1. Pulsars with X-ray and/or TeV PWNe

#	PSR	PWN*	VHE src. [†]	$\log \dot{E}$ [erg/s]	$\log \tau$ [yr]	d^{**} kpc	Rad./ H_α /GeV ‡
1	J0537-6910	N157B	...	38.68	3.70	50	Y/N/N
2	B0531+21	Crab	H J0534+220	38.66	3.09	2	Y/N/Y
3	J2022+3842	G76.9+1.0	...	38.30	3.95	8	Y/N/N
4	B0540-69	N158A	...	38.17	3.22	50	Y/N/N
5	J1813-1749	G12.82-0.02	H J1813-178 [?]	37.83	3.66	4.5	N/N/P
6	J1400-6325	G310.6-1.6	...	37.71	4.10	6	Y/N/N
7	J1833-1034	G21.50-0.89	H J1833-105	37.52	3.69	4.8	Y/N/Y
8	J0205+6449	3C 58	...	37.43	3.73	3.2	Y/N/Y
9	J2229+6114	G106.65+2.96	V J2228+609	37.35	4.02	3	Y/N/Y
10	B1509-58	Jellyfish	H J1514-591	37.25	3.19	5	P/N/N
11	J1617-5055	G332.50-0.28	H J1616-508 [?]	37.20	3.91	6.5	N/N/P
12	J1124-5916	G292.04+1.75	...	37.07	3.46	6	Y/N/Y
13	J1930+1852	G54.10+0.27	V J1930+188	37.06	3.46	6.2	Y/N/N
14	J1420-6048	G313.54+0.23	H J1420-607	37.02	4.11	5.6	P/N/N
15	J1846-0258	Kes 75	H J1846-029	36.91	2.86	6 ^{??}	Y/N/N
16	B0833-45	Vela	H J0835-455	36.84	4.05	0.29 ^P	Y/N/N
17	J1811-1925	G11.18-0.35	...	36.81	4.37	5	Y/N/N
18	J1838-0655	G25.24-0.19	H J1837-069	36.74	4.36	7	N/N/N
19	J1418-6058	Rabbit	H J1418-609	36.69	4.00	3 [?]	Y/N/Y
20	J1856+0245	G36.01+0.06 [?]	H J1857+026	36.66	4.32	9	N/N/N
21	B1951+32	G68.77+2.82	...	36.57	5.03	2.5	Y/Y/Y
22	J1826-1256	Eel	...	36.55	4.15	7 [?]	P/N/Y
23	J2021+3651	G75.23+0.12	M J2019+37 [?]	36.53	4.23	4	N/N/Y
24	B1706-44	G343.10-2.69	H J1708-443	36.53	4.24	2	Y/N/Y
25	J1357-6429	G309.92-2.51	H J1357-645	36.49	3.86	2.5	P/N/N
26	J1913+1011	G44.48-0.17 [?]	H J1912+101	36.46	5.23	4.5	N/N/N
27	J1907+0602	G40.16-0.89 [?]	H J1908+063 [?]	36.45	4.28	3.2	N/N/Y
28	B1823-13	G18.00-0.69	H J1825-137	36.45	4.33	4	N/N/N
29	B1757-24	Duck	...	36.41	4.19	5	Y/N/N
30	J1016-5857	G284.08-1.88	...	36.41	4.32	3	N/N/N
31	J1747-2958	Mouse	...	36.40	4.41	5	Y/N/Y
32	J1119-6127	G292.15-0.54	H J1119-615 [?]	36.37	3.21	8.4	N/N/N
33	B1800-21	G8.40+0.15	H J1804-216 [?]	36.34	4.20	4	N/N/P
34	B1046-58	G287.42+0.58	...	36.30	4.31	3	N/N/Y
35	J1809-1917	G11.09+0.08	H J1809-193	36.25	4.71	3.5	P/N/N
36	J1301-6305	G304.10-0.24	H J1303-631 [?]	36.22	4.04	7	N/N/N
37	J1718-3825	G348.95-0.43	H J1718-385 [?]	36.11	4.95	4	N/N/Y
38	J1531-5610	G323.89+0.03	...	35.96	4.99	3	N/N/N
39	J1509-5850	G319.97-0.62	...	35.71	5.19	4	P/N/Y
40	J1857+0143	G35.17-0.57 [?]	H J1858+020 [?]	35.65	4.85	5.5	N/N/N
41	J0007+7303	CTA1	...	35.65	4.15	1.4	N/N/Y
42	B1853+01	G34.56-0.50	...	35.63	4.31	3	Y/N/N
43	J1809-2332	Taz	...	35.60	4.36	2	Y/N/N
44	J1958+2846	G65.89-0.37 [?]	M J1954+28	35.58	4.32	2 [?]	N/N/Y
45	J1702-4128	G344.74+0.12	H J1702-420 [?]	35.53	4.74	5	N/N/N
46	J0729-1448	G230.39-1.42	...	35.45	4.54	4	N/N/N
47	J2032+4127	G80.22+1.02	He J2032+4130	35.43	5.04	1.7	N/N/Y
48	J1740+1000	G34.01+20.27	...	35.36	5.06	1.4	N/N/N

TABLE 1. Pulsars with X-ray and/or TeV PWNe (continued)

#	PSR	PWN*	VHE src. [†]	$\log \dot{E}$ [erg/s]	$\log \tau$ [yr]	d^{**} kpc	Rad./ H_α /GeV [‡]
49	J0631+1036	G201.22+0.45 [?]	M J0630+10 [?]	35.24	4.64	3.6	N/N/Y
50	B1957+20	G59.20–4.70	...	35.20	9.18	2.5	N/Y/N
51	J0633+0632	G205.10–0.93	...	35.08	4.77	1.5 [?]	N/N/Y
52	J1740–3015	G358.29+0.24 [?]	H J1741–302	34.91	4.31	3	N/N/N
53	J0538+2817	G179.72–1.69	...	34.69	5.79	1.47 ^P	N/N/N
54	B0355+54	Mushroom	...	34.66	5.75	1.04 ^P	N/N/N
55	J0633+1746	Geminga	M J0632+17 [?]	34.51	5.53	0.25 ^P	N/N/Y
56	J1745–3040	G358.55–0.96 [?]	H 1745–305 [?]	33.93	5.74	2	N/N/N
57	J1502–5828	G319.39+0.13 [?]	H J1503–582 [?]	33.68	5.46	8	N/N/N
58	B1929+10	G47.38–3.88	...	33.59	6.49	0.36 ^P	P/N/N
59	B2224+65	Guitar	...	33.07	6.05	1.5	N/Y/N

* PWN name or galactic coordinates. The superscript [?] mark the cases in which no X-ray PWN has been reported, but there are TeV PWN candidates nearby.

[†] TeV sources in the vicinity of the PSR/PWN. ‘H’, ‘V’, ‘M’ and ‘He’ stand for HESS, VERITAS, Milagro and HEGRA. The superscript [?] marks questionable associations.

** Our best guess for the pulsar distance, used to scale the distance-dependent parameters in Table 2. The superscript ^P marks the distances determined from parallax measurements; the most uncertain distances (e.g., when even dispersion measure is unknown) are marked by [?]. For Kes 75 the distance (marked by ^{??}) is rather uncertain, ranging from 5.1–7.5 kpc ([3]) to ~ 10.6 kpc ([4]).

[‡] Is the PWN detected in radio/ H_α , and PSR/PWN in GeV γ -rays? P = ‘possibly’.

down timescale; e.g., [1]). This picture is further complicated by environmental effects and pulsar motion. For instance, the ambient pressure that confines a slowly-moving PWN, is much greater in a star-forming region than in low-density regions above the Galactic plane; high-speed pulsars are accompanied by long tails with higher bulk flow velocities compared to more isotropic PWNe around slowly-moving pulsars; pressure gradients inside a supernova remnant or interaction with its reverse shock can affect the PWN shape. In addition, the ambient radio/IR radiation density may vary and affect the properties of the IC radiation emitted by the pulsar wind. In many cases, significant offsets between the centroid of the extended TeV source and the neighboring pulsar’s position may be attributed to the interaction with the asymmetric reverse shock or to a locally non-uniform distribution of the ambient matter/radiation. The large sizes of these TeV sources and the large offsets may sometimes lead to false associations with pulsars, especially if there is no preferential extension of the X-ray PWN toward the TeV source center.

The X-ray and TeV spectra of PWNe are often approximated by power-law (PL) models with different slopes. If the electron spectral energy distribution (SED) can be approximated by a single PL, $dN(\epsilon) \propto \epsilon^{-p} d\epsilon$, then both the synchrotron (X-ray) and IC (TeV) spectra should have the same slopes, $F_\nu \propto \nu^{-\Gamma+1}$, where the photon index $\Gamma = (p + 1)/2$. However, one can see from Table 2 that the spectra of X-ray PWNe are systematically harder than those of their TeV counterparts, which can be attributed to the evolution of the electron SED. Indeed, *Chandra* observations of bright, well-resolved PWNe have shown that the synchrotron spectrum varies significantly with the distance from the pulsar (due to the radiation and expansion energy losses), and therefore a single PL approximation to the X-ray spectrum becomes inapplicable if a large enough volume

TABLE 2. Properties of the X-ray/TeV PWNe listed in Table 1

#	$N_{\text{H},22}^*$	$\log L_{\text{X}}^\dagger$ [erg/s]	Γ_{X}	$\log L_{\gamma}^{**}$ [erg/s]	Γ_{γ}^\ddagger	l_{X}^\S pc	l_{γ}^\P pc	Δ^\parallel arcmin	Refs. ^{††}
1	0.5	36.04 ± 0.01	2.20 ± 0.05	1.4	[5]
2	0.32	37.28 ± 0.01	2.12 ± 0.01	34.51 ± 0.06	2.63 ± 0.20	1.2	< 2	< 0.5	[6, 7, 8]
3	1.3	32.58 ± 0.12	0.9 ± 0.5	0.4	[9]
4	0.46	37.01 ± 0.01	1.85 ± 0.10	1.4	[10]
5	10	32.90 ± 0.25	$0.4_{-0.7}^{+0.4}$	34.34 ± 0.14	2.09 ± 0.21	2.0	6	< 0.5	[11, 12, 13]
6	2.1	34.99 ± 0.04	1.83 ± 0.09	2.3	[14]
7	2.3	35.36 ± 0.01	1.89 ± 0.02	33.63 ± 0.12	2.08 ± 0.22	1.0	< 5	< 1	[15, 16]
8	0.43	33.94 ± 0.01	2.02 ± 0.01	1.2	[17]
9	0.5	32.94 ± 0.01	1.3 ± 0.1	33.63 ± 0.20	2.3 ± 0.4	0.4	26	24	[18, 19]
10	0.8	34.60 ± 0.03	1.65 ± 0.05	34.86 ± 0.12	2.27 ± 0.2	4.5	24	2.4	[20, 21]
11	3.5	33.79 ± 0.02	1.2 ± 0.2	34.78 ± 0.06	2.35 ± 0.21	0.6	60	10	[22, 12]
12	0.37	34.71 ± 0.03	1.7 ± 0.5	0.2	[23]
13	1.9	34.46 ± 0.01	1.99 ± 0.03	33.88 ± 0.20	2.3 ± 0.4	1.5	< 11	< 3	[24, 19]
14	5.4	33.15 ± 0.11	0.5 ± 1.2	34.60 ± 0.07	2.17 ± 0.12	0.4	11	3.3	[25, 26]
15	4.0	35.19 ± 0.02	2.03 ± 0.02	33.87 ± 0.09	2.26 ± 0.15	2.8	< 6	< 1	[27]
16	0.02	32.11 ± 0.03	1.4 ± 0.1	32.14 ± 0.22	$1.45 \pm 0.22^?$	0.1	5	30	[28, 29, 30]
17	3.1	34.00 ± 0.09	1.5 ± 0.2	1.0	[31]
18	4.0	33.47 ± 0.14	0.8 ± 0.3	34.91 ± 0.18	2.27 ± 0.21	2.0	28	3	[32, 12]
19	2.3	33.55 ± 0.02	1.7 ± 0.1	33.91 ± 0.07	2.22 ± 0.12	1.5	8	3.5	[25, 26]
20	$\lesssim 2$	35.16 ± 0.11	2.39 ± 0.08	1.7	40	6	[33, 34]
21	0.34	32.62 ± 0.01	1.76 ± 0.03	0.4	[35, 36]
22	2.0	32.41 ± 0.05	1.27 ± 0.40	0.3	[37]
23	0.7	33.08 ± 0.07	1.7 ± 0.3	33.09 ± 0.50	[2.6]	0.8	< 140	18	[38, 39]
24	0.5	32.58 ± 0.02	1.8 ± 0.1	33.87 ± 0.13	2.00 ± 0.22	0.2	23	14	[40, 41]
25	0.23	31.70 ± 0.07	1.28 ± 0.21	33.77 ± 0.20	2.2 ± 0.2	0.1	20	8	[42]
26	$\lesssim 2$	< 31.22	...	34.19 ± 0.19	2.7 ± 3.6	...	60	12	[43]
27	$\lesssim 2$	34.22 ± 0.22	2.10 ± 0.21	...	37	16	[44]
28	1.0	32.50 ± 0.05	1.3 ± 0.4	35.05 ± 0.10	$2.26 \pm 0.2^?$	0.2	70	10	[45, 46, 47]
29	4.4	33.20 ± 0.14	2.5 ± 0.3	0.5	[48]
30	[1.2]	32.30 ± 0.11	1.5 ± 0.2	0.1	[49]
31	3.0	34.70 ± 0.05	2.0 ± 0.2	0.5	[50]
32	1.6	33.00 ± 0.10	1.5 ± 0.3	34.20 ± 0.30	> 2.2	0.5	30	6	[51, 52]
33	1.4	32.20 ± 0.05	1.6 ± 0.3	34.30 ± 0.08	2.72 ± 0.21	0.2	58	10	[53, 54, 12]
34	[0.4]	31.82 ± 0.04	1.0 ± 0.2	0.2	[55]
35	0.7	32.59 ± 0.03	1.4 ± 0.1	34.29 ± 0.11	2.20 ± 0.22	0.2	40	8	[56, 57]
36	[1.1]	32.16 ± 0.50	...	34.76 ± 0.08	2.44 ± 0.21	2.0	39	11	[58]
37	0.7	32.60 ± 0.10	1.9 ± 0.2	33.74 ± 0.30	$0.7 \pm 0.6^?$	2.0	7	3	[59, 57]
38	$\lesssim 2$	31.03 ± 0.5	0.1
39	2.1	32.12 ± 0.13	1.8 ± 0.3	0.4	[60]
40	$\lesssim 2$	33.82 ± 0.25	2.17 ± 0.23	...	< 13	...	[34]
41	[0.3]	31.38 ± 0.20	1.1 ± 0.6	0.1	[61]
42	2.0	31.93 ± 0.13	2.1 ± 1.0	0.4	[62]
43	0.3	31.54 ± 0.30	1.5 ± 0.6	0.3
44	$\lesssim 1$	32.00 ± 0.50	[2.6]	< 40	[39]
45	[1.1]	31.60 ± 0.50	...	34.30 ± 0.11	2.31 ± 0.23	0.2	50	30	[12]
46	[0.3]	31.20 ± 0.50	0.05
47	[1.5]	31.53 ± 0.10	[1.5]	32.97 ± 0.09	1.9 ± 0.3	0.5	6	4	[63, 64, 65]
48	[0.1]	31.11 ± 0.10	1.5 ± 0.3	0.8	[60]

TABLE 2. Properties of the X-ray/TeV PWNe listed in Table 1

#	$N_{\text{H},22}^*$	$\log L_X^\dagger$ [erg/s]	Γ_X	$\log L_\gamma^{**}$ [erg/s]	Γ_γ^\ddagger	l_X^\S pc	l_γ^\P pc	Δ^\parallel arcmin	Refs. ^{††}
49	$\gtrsim 0.6$	< 31.15	...	32.64 ± 0.50	[2.6]	...	< 180	...	[39, 66]
50	0.1	30.81 ± 0.18	1.6 ± 0.5	0.1	[67]
51	$\gtrsim 0.04$	1.5	[68]
52	$\gtrsim 1.5$	32.82 ± 0.15	2.78 ± 0.31	...	22	12	[69]
53	0.25	31.04 ± 0.10	3.3 ± 0.5	0.2	[70, 71]
54	0.6	31.19 ± 0.03	1.5 ± 0.1	0.1	[72]
55	0.03	29.71 ± 0.07	1.0 ± 0.2	30.22 ± 0.50	[2.6]	0.02	10	< 30	[73, 39]
56	$\gtrsim 1.3$	< 31	...	~ 33.01	1.82 ± 0.35	...	6	7	[69]
57	$\gtrsim 2$	34.66 ± 0.60	2.4 ± 0.44	...	70	...	[69]
58	0.17	29.63 ± 0.01	1.7 ± 0.6	0.05	[74]
59	0.2	29.5 ± 0.5	[1.5]	0.07	[75]

* Hydrogen column density (in units of 10^{22} cm^{-2}) obtained from spectral fits to the PWN spectra or estimated from the pulsar’s dispersion measure assuming 10% interstellar medium ionization (in square brackets for the latter case). In a few cases upper limits are given based on the galactic HI column density.

† Logarithm of PWN luminosity in the 0.5–8 keV band. The quoted errors are purely statistical, they do not include the distance errors. For bright PWNe (e.g., ## 2, 8, 16), we quote the luminosity of the PWN “core” restricted to the torus/arcs regions. For the PWNe with extended tails (## 39, 42, 48, 53, 54, 55, 58) we quote only the luminosity of the bright “bullet” component. For ## 36, 45 and 46, faint extended emission is seen around the pulsar but its luminosity is very uncertain; we use ± 0.50 dex as a conservative estimate for the uncertainty.

** Logarithm of PWN (or candidate) luminosity in the 1–10 TeV band.

‡ Photon index of TeV spectrum determined from a power-law model. The fits are not good (e.g., an exponential cutoff is required or the spectral slope is nonuniform) in the cases marked by the superscript [?]. The values in square brackets were assumed for estimating L_γ .

§ Size of X-ray PWN “core” in which the PWN X-ray properties listed in this table were measured.

¶ Size of TeV source. If the source is unresolved, we quote the upper limit on l_γ .

∥ Offset between the X-ray and TeV components.

†† The PWN/PSR X-ray properties listed here were measured by ourselves (except for ## 2, 5, 6, 10, 37, 47, 49 and 51), but we cite recent relevant papers when available.

around the pulsar is considered. Also, the IC spectrum may deviate from a PL at large energies due to the intrinsic upper boundary of the electron SED, or due to the cooling effects. In addition to the spectral differences caused by the cooling and boundary effects, one should keep in mind that while the intensity of the synchrotron component depends on the magnetic field strength, the IC intensity depends on the ambient radiation density instead. Therefore, there is no reason to expect direct proportionality between the X-ray and TeV fluxes of a particular PWN, and indeed we see little correlation between the X-ray and TeV luminosities (Fig. 1, panel A). Yet, the X-rays, observed from the innermost PWN region, and TeV γ -rays, produced throughout the entire PWN volume, can be related in a model that takes into account the pulsar wind history (e.g., the evolution of \dot{E} and the PWN size), its spatially varying properties, and local radiation density. While measured from spatially different regions of a PWN, the X-ray and TeV luminosities in Table 2 still can be used to test such models as long as the observed values are compared with the model values calculated for appropriate PWN zones and time intervals. There have been a number of analytical models that take into account either the spatial dependence (e.g., [76, 77]) or time-dependence (e.g., [78, 79]) of the PWN properties but rarely both ([80]).

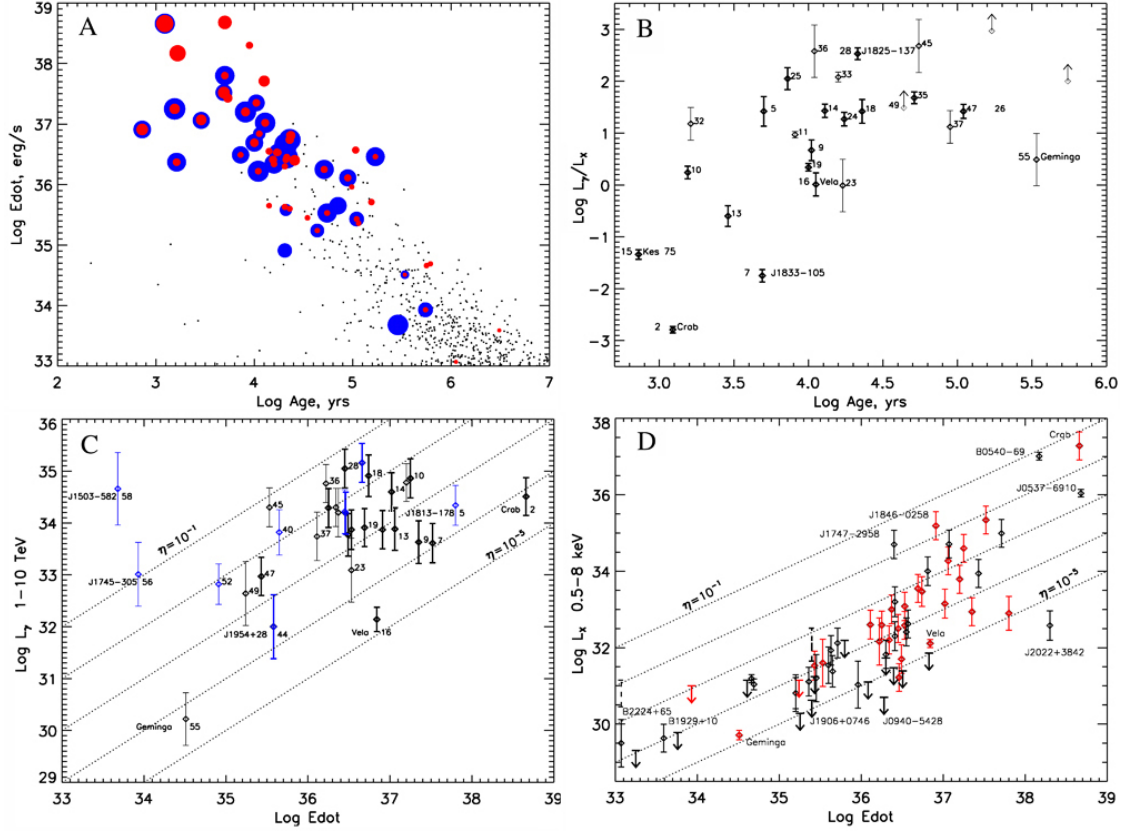


FIGURE 1. (A) Filled circles are X-ray (red) and TeV (blue) detected PWNe or PWN candidates. Larger circle sizes correspond to higher luminosities. The small black dots denote the pulsars from the ATNF catalog ([81]). (B) Ratio of the TeV to X-ray luminosities vs. pulsar’s spin-down age. Here and in panel C the thin error bars mark questionable associations. (C) TeV luminosities of PWNe and PWN candidates vs. pulsar’s \dot{E} . The blue error bars mark TeV objects without X-ray counterparts. Here and in panel D the luminosity uncertainties include 50% systematic uncertainty assigned to the distances unless the pulsar is in LMC or its parallax has been measured. (D) X-ray luminosities of PWNe vs. \dot{E} . The red error bars denote X-ray PWNe with TeV counterparts. The lines of constant radiative efficiency ($\eta \equiv L_{X,\gamma}/\dot{E}$) are plotted in panels C and D.

In panels C and D of Figure 1 we show the dependences of the luminosities L_X and L_γ on \dot{E} . As expected, we do not see an obvious correlation between L_γ and \dot{E} , which likely reflects the fact that the TeV luminosity depends on the history of the pulsar spin-down rather than on the current \dot{E} . An additional scatter is expected due to the differences in the local IR background and the uncertain distances. Most of the 1–10 TeV luminosities cluster in the range of 10^{33} – 10^{35} erg s $^{-1}$, a much narrower span than that attained by the X-ray luminosities shown in another panel. The L_X versus \dot{E} plot does show some correlation between the two; however, the more objects are included the larger the scatter becomes, weakening the correlation. It seems very unlikely that a factor of 10^4 scatter at a given \dot{E} could be explained by varying environment (e.g., ambient pressure) or differences in pulsar velocities. Some “hidden” pulsar parameters (e.g., the angle between the rotation and magnetic axis, or the topology of the NS magnetic field) may instead govern the efficiency of the magnetic-to-kinetic energy conversion and, as a result, the X-ray efficiencies of PWNe (see also [2]). In Figure 1 (panel B) we also

plot the distance-independent L_γ/L_X as a function of spin-down age τ , which shows a hint of positive correlation between the two, at younger ages. This correlation can be explained by the correlation between L_X and \dot{E} (hence the anti-correlation between L_X and τ). These results are in general agreement with the recent findings of [82] based on a smaller sample of PWNe. At $\log \tau \gtrsim 4.5$ the dependence of L_γ/L_X on τ appears to level off as expected from the simple model of [82]. This trend, however, shows a large scatter, which might be attributed to the magnetic and radiation fields being different for different objects.

To conclude, multiwavelength observations of PWNe are crucial because they provide identifications for VHE sources and reveal the true energetics and composition of pulsar winds. In addition to X-ray and TeV observations, there is an opportunity to detect the IC PWN component with *Fermi* in GeV, where even old objects are expected to exhibit uncooled IC spectrum which should be more directly linked to the radio synchrotron component. The data accumulation must be complemented by development of multi-zone models of PWN evolution, essential for understanding the role of pulsar winds in seeding the Galaxy with energetic particles and magnetic fields.

ACKNOWLEDGMENTS

We would like to thank Wenwu Tian for providing updated distances for several sources. The authors acknowledge support from NASA grants NNX09AC81G and NNX09AC84G, and *Chandra* award AR8-9009X. This material is also based upon work supported by the National Science Foundation under Grants No. 0908733 and 0908611.

REFERENCES

1. B. M. Gaensler, and P. O. Slane, *Ann. Rev. A&A* **44**, 17–47 (2006).
2. O. Kargaltsev, and G. G. Pavlov, “Pulsar Wind Nebulae in the Chandra Era,” in *AIP Conf. Proc.*, edited by C. Bassa, Z. Wang, A. Cumming, & V. M. Kaspi, 2008, vol. 983, pp. 171–185.
3. D. A. Leahy, and W. W. Tian, *A&A* **480**, L25–L28 (2008).
4. Y. Su, Y. Chen, J. Yang, et al., *ApJ* **694**, 376–386 (2009).
5. Y. Chen, Q. D. Wang, E. V. Gotthelf, et al., *ApJ* **651**, 237–249 (2006).
6. K. Mori, D. N. Burrows, J. J. Hester, et al., *ApJ* **609**, 186–193 (2004).
7. R. Willingale, B. Aschenbach, R. G. Griffiths, et al., *A&A* **365**, L212–L217 (2001).
8. F. Aharonian, et al., *A&A* **457**, 899–915 (2006).
9. Z. Arzoumanian, *talk at Supernova Remnants and PWNe in the Chandra Era, Boston, MA* (2009).
10. P. Kaaret, H. L. Marshall, T. L. Aldcroft, et al., *ApJ* **546**, 1159–1167 (2001).
11. D. J. Helfand, E. V. Gotthelf, J. P. Halpern, et al., *ApJ* **665**, 1297–1303 (2007).
12. F. Aharonian, et al., *ApJ* **636**, 777–797 (2006).
13. E. V. Gotthelf, and J. P. Halpern, *ApJL* **700**, L158–L161 (2009).
14. M. Renaud, V. Marandon, E. V. Gotthelf, et al., *arXiv:0910.3074* (2009).
15. S. Safi-Harb, I. M. Harrus, R. Petre, et al., *ApJ* **561**, 308–320 (2001).
16. A. Djannati-Ataï, O. C. de Jager, R. Terrier, et al., “New Companions for the lonely Crab? ,” in *International Cosmic Ray Conf. Proc.*, 2008, vol. 2, pp. 823–826.
17. P. Slane, D. J. Helfand, E. van der Swaluw, et al., *ApJ* **616**, 403–413 (2004).
18. J. P. Halpern, F. Camilo, E. V. Gotthelf, et al., *ApJL* **552**, L125–L128 (2001).
19. E. Aliu, *talk at Supernova Remnants and PWNe in the Chandra Era, Boston, MA* (2009).
20. B. M. Gaensler, J. Arons, V. M. Kaspi, et al., *ApJ* **569**, 878–893 (2002).
21. F. Aharonian, et al., *A&A* **435**, L17–L20 (2005).

22. O. Kargaltsev, G. G. Pavlov, and J. A. Wong, *ApJ* **690**, 891–901 (2009).
23. J. P. Hughes, P. O. Slane, D. N. Burrows, et al., *ApJL* **559**, L153–L156 (2001).
24. F. J. Lu, Q. D. Wang, B. Aschenbach, et al., *ApJL* **568**, L49–L52 (2002).
25. C.-Y. Ng, M. S. E. Roberts, and R. W. Romani, *ApJ* **627**, 904–909 (2005).
26. F. Aharonian, et al., *A&A* **456**, 245–251 (2006).
27. D. J. Helfand, B. F. Collins, and E. V. Gotthelf, *ApJ* **582**, 783–792 (2003).
28. G. G. Pavlov, O. Y. Kargaltsev, D. Sanwal, et al., *ApJL* **554**, L189–L192 (2001).
29. D. J. Helfand, E. V. Gotthelf, and J. P. Halpern, *ApJ* **556**, 380–391 (2001).
30. F. Aharonian, et al., *A&A* **448**, L43–L47 (2006).
31. M. S. E. Roberts, C. R. Tam, V. M. Kaspi, et al., *ApJ* **588**, 992–1002 (2003).
32. E. V. Gotthelf, and J. P. Halpern, *ApJ* **681**, 515–521 (2008).
33. J. W. T. Hessels, D. J. Nice, B. M. Gaensler, et al., *ApJL* **682**, L41–L44 (2008).
34. F. Aharonian, et al., *A&A* **477**, 353–363 (2008).
35. D.-S. Moon, J.-J. Lee, S. S. Eikenberry, et al., *ApJL* **610**, L33–L36 (2004).
36. X. H. Li, F. J. Lu, and T. P. Li, *ApJ* **628**, 931–937 (2005).
37. M. Roberts, C. Brogan, and M. Lyutikov, *BAAS* **38**, 997 (2007).
38. J. W. T. Hessels, M. S. E. Roberts, S. M. Ransom, et al., *ApJ* **612**, 389–397 (2004).
39. A. A. Abdo, et al., *ApJL* **700**, L127–L131 (2009).
40. R. W. Romani, C.-Y. Ng, R. Dodson, et al., *ApJ* **631**, 480–487 (2005).
41. S. Hoppe, E. de Oña-Wilhemí, B. Khélifi, et al., *arXiv:0906.5574* (2009).
42. V. E. Zavlin, *ApJL* **665**, L143–L146 (2007).
43. F. Aharonian, et al., *A&A* **484**, 435–440 (2008).
44. F. Aharonian, et al., *A&A* **499**, 723–728 (2009).
45. B. M. Gaensler, N. S. Schulz, V. M. Kaspi, et al., *ApJ* **588**, 441–451 (2003).
46. G. G. Pavlov, O. Kargaltsev, and W. F. Brisken, *ApJ* **675**, 683–694 (2008).
47. F. Aharonian, et al., *A&A* **460**, 365–374 (2006).
48. V. M. Kaspi, E. V. Gotthelf, B. M. Gaensler, et al., *ApJL* **562**, L163–L166 (2001).
49. F. Camilo, B. M. Gaensler, E. V. Gotthelf, et al., *ApJ* **616**, 1118–1123 (2004).
50. B. M. Gaensler, E. van der Swaluw, F. Camilo, et al., *ApJ* **616**, 383–402 (2004).
51. M. Gonzalez, and S. Safi-Harb, *ApJL* **591**, L143–L146 (2003).
52. A. Djannati-Atai, *talk at Supernova Remnants and PWNe in the Chandra Era, Boston, MA* (2009).
53. O. Kargaltsev, G. G. Pavlov, and G. P. Garmire, *ApJ* **660**, 1413–1423 (2007).
54. O. Kargaltsev, G. G. Pavlov, and G. P. Garmire, *ApJ* **670**, 643–654 (2007).
55. M. E. Gonzalez, V. M. Kaspi, M. J. Pivovarov, et al., *ApJ* **652**, 569–575 (2006).
56. O. Kargaltsev, and G. G. Pavlov, *ApJ* **670**, 655–667 (2007).
57. F. Aharonian, et al., *A&A* **472**, 489–495 (2007).
58. F. Aharonian, et al., *A&A* **439**, 1013–1021 (2005).
59. J. A. Hinton, S. Funk, S. Carrigan, et al., *A&A* **476**, L25–L28 (2007).
60. O. Kargaltsev, Z. Misanovic, G. G. Pavlov, et al., *ApJ* **684**, 542–557 (2008).
61. J. P. Halpern, E. V. Gotthelf, F. Camilo, et al., *ApJ* **612**, 398–407 (2004).
62. R. Petre, K. D. Kuntz, and R. L. Shelton, *ApJ* **579**, 404–410 (2002).
63. F. Camilo, P. S. Ray, S. M. Ransom, et al., *ApJ* **705**, 1–13 (2009).
64. F. Aharonian, et al., *A&A* **393**, L37–L40 (2002).
65. R. Mukherjee, E. V. Gotthelf, and J. P. Halpern, *Astrophys. Space Sci.* **309**, 29–33 (2007).
66. P. Weltevrede, A. A. Abdo, M. Ackermann, et al., *ApJ* **708**, 1426–1441 (2010).
67. B. W. Stappers, B. M. Gaensler, V. M. Kaspi, et al., *Science* **299**, 1372–1374 (2003).
68. N. Kawai, *talk at Fermi Symposium, Washington, DC* (2009).
69. O. Tibolla, R. C. G. Chaves, O. de Jager, et al., *arXiv:0907.0574* (2009).
70. R. W. Romani, and C.-Y. Ng, *ApJL* **585**, L41–L44 (2003).
71. C.-Y. Ng, R. W. Romani, W. F. Brisken, et al., *ApJ* **654**, 487–493 (2007).
72. K. E. McGowan, W. T. Vestrand, J. A. Kennea, et al., *ApJ* **647**, 1300–1308 (2006).
73. G. G. Pavlov, D. Sanwal, and V. E. Zavlin, *ApJ* **643**, 1146–1150 (2006).
74. Z. Misanovic, G. G. Pavlov, and G. P. Garmire, *ApJ* **685**, 1129–1142 (2008).
75. C. Y. Hui, and W. Becker, *A&A* **467**, 1209–1214 (2007).
76. C. F. Kennel, and F. V. Coroniti, *ApJ* **283**, 694–709 (1984).
77. C. F. Kennel, and F. V. Coroniti, *ApJ* **283**, 710–730 (1984).

78. R. A. Chevalier, *ApJL* **539**, L45–L48 (2000).
79. J. D. Gelfand, P. O. Slane, and W. Zhang, *ApJ* **703**, 2051–2067 (2009).
80. E. Amato, M. Salvati, R. Bandiera, et al., *A&A* **359**, 1107–1110 (2000).
81. R. N. Manchester, G. B. Hobbs, A. Teoh, et al., *AJ* **129**, 1993–2006 (2005).
82. F. Mattana, M. Falanga, D. Götz, et al., *ApJ* **694**, 12–17 (2009).